Nuclear Instruments and Methods in Physics Research A 660 (2011) 138–146

Contents lists available at SciVerse ScienceDirect

Nuclear Instruments and Methods in Physics Research A

journal homepage: www.elsevier.com/locate/nima

The BTFEL, an infrared free-electron laser amplifier based on a new-design short-period superconducting tape undulator

M. Yoon [a,b], D. Filippetto [a], C.F. Papadopoulos [a], C. Pellegrini [c], G. Penn [a], S. Prestemon [a], F. Sannibale [a,*]

[a] Lawrence Berkeley National Laboratory, 1 Cyclotron Road, Berkeley, CA 94720, USA
[b] Department of Physics, Postech, Hyoja-dong, Pohang, Gyeongbuk 790-784, Republic of Korea
[c] Department of Physics, University of California, Los Angeles, CA 90095, USA

ARTICLE INFO

Article history:
Received 6 July 2011
Received in revised form
14 September 2011
Accepted 23 September 2011
Available online 3 October 2011

Keywords:
Infrared radiation
FEL
SASE
Short period undulator

ABSTRACT

The development of undulator technologies capable of generating sub-cm undulator periods is assuming an increasing importance in X-ray free electron laser (FEL) applications. Indeed, such devices jointly with the high brightness electron beams already demonstrated at operating facilities would allow for lower energy, more compact electron linacs with a beneficial impact on the size and cost of X-ray FEL facilities.

A novel design super-conducting undulator is being developed at the Lawrence Berkeley National Laboratory (LBNL) with the potential of sub-cm periods with reasonably large undulator parameter and gap. The potential and capability of such undulator technology need to be experimentally demonstrated.

In this paper, the possibility of constructing an infrared FEL by combining the new undulator with the high brightness beam from the APEX injector facility at LBNL is investigated.

Calculations show that the resulting FEL, when operated in self-amplified-spontaneous-emission mode, is expected to deliver a saturated power of almost a MW within a $\sim$4 m undulator length, in a single-spike of coherent radiation at $\sim$2 μm wavelength.

It will be also shown that the small-period of the undulator associated with the relatively low energy of the APEX beam, forces the FEL to operate in a regime with unusual and interesting characteristics. The alternative option of laser seeding the FEL is also briefly examined, showing the potential to reduce the saturation length even further.

1. Introduction

The formidable success of LCLS at SLAC, the first hard X-ray free electron laser (FEL) [1], demonstrated the capability of such a type of facility to generate laser-like emission at sub-nanometer wavelengths. In order to achieve the electron beam quality required by the FEL process, multi-GeV electron beams are necessary, requiring high energy linacs and making such facilities large and expensive. On the other hand, LCLS results have already demonstrated the potential for transverse normalized emittances ε_n low enough to match the 'photon emittance' requirements $\varepsilon_n/\beta\gamma \sim \lambda/4\pi$ at lower beam energies if an undulator with the proper period λ_u can be manufactured to simultaneously satisfy the undulator resonance condition $\lambda = \lambda_u/2\gamma^2(1+K^2/2)$. In the above expressions, β is the electron velocity in speed of light units, γ the electron energy in rest mass units, λ the radiation wavelength, and $K = eB_u\lambda_u/2\pi mc$ is the dimensionless undulator parameter with B_u the peak magnetic field on axis, m the electron rest mass, and c the speed of light in vacuum.

Present undulator technology limits the shortest undulator period to $\sim$1.5 cm, and any progress toward shortening such a quantity will have a direct beneficial impact by reducing the size and cost of X-ray FEL facilities.

In order to respond to this need, research is undergoing at the Lawrence Berkeley National Laboratory (LBNL) to develop a sub-centimeter period, high-temperature super-conducting tape undulator with planar geometry utilizing YBCO material [2–4].

Also, in a parallel research activity at LBNL, the Advanced Photo-injector EXperiment (APEX), a compact beam test facility, is currently under construction [5–7]. The primary purpose of this facility is to demonstrate the capability of a novel scheme electron gun to generate, at high repetition rate (1 MHz and beyond), electron beams with brightness and characteristics compatible with the operation of X-ray free electron lasers (FEL).

The core of the injector gun consists of by a normal-conducting copper RF cavity resonating in the VHF band (187 MHz), and capable to run in constant wave (CW) mode. Such a cavity combined with

* Corresponding author. Tel.: +1 510 486 5924; fax: +1 510 486 4960.
E-mail addresses: moohyun@postech.edu (M. Yoon), fsannibale@lbl.gov (F. Sannibale).

0168-9002/$ - see front matter © 2011 Elsevier B.V. All rights reserved.
doi:10.1016/j.nima.2011.09.042

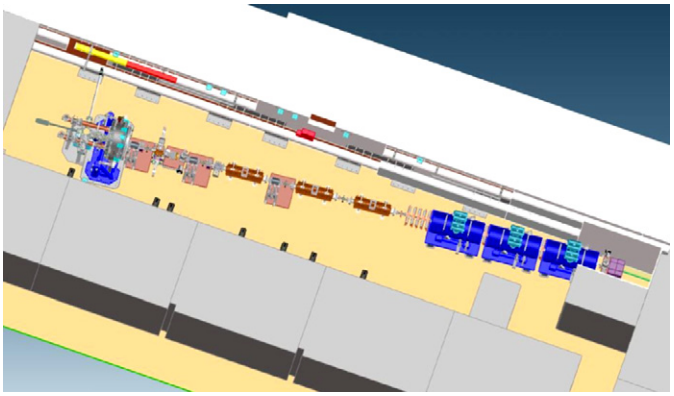

Fig. 1. APEX facility layout. The electron gun is on the top-left part of the figure while the dark cylinders in the bottom-left are the three undulator cryostats. The total length of the shielded area is about 15 m.

high quantum efficiency (QE) photo-cathodes will allow to generate up to ~ 1 nC bunches at 1 MHz repetition rate using commercially available lasers.

APEX will also include a small normal conducting 1.3 GHz pulsed linac to accelerate the beam up to few tens of MeV, so to reduce space charges forces down to a level sufficient to measure the actual brightness performance of the electron gun. While the beam at the gun energy (0.75 MeV) will be run at full repetition rate, at the linac energy, the operation will be limited instead to few Hz due to radiation shielding limitations of the Beam Test Facility (BTF), the pre-existing shielded area where APEX is located. Fig. 1 shows the CAD view of the APEX injector.

The idea described in this paper is to test and demonstrate the promising super-conducting tape undulator technology with the APEX beam. When such an undulator is coupled with the APEX injector, an infrared (IR) FEL with a number interesting and unusual characteristics is obtained. We refer to this configuration of as the Beam Test facility Free Electron Laser (BTFEL).

In Section 2 of the paper, the peculiar FEL regime of such a system is qualitatively described. In Section 3, we list the BTFEL parameters, including the electron beam properties and the predicted radiation in self-amplified spontaneous emission (SASE) mode [8,9], and give brief descriptions of the characteristics of the super-conducting tape undulator and of the optical function matching inside the undulators in the presence of space charge effects. In Section 4, the FEL performance calculated in Section 3 is compared by time-dependent FEL simulations. Finally, before Section 6, the possibility of laser seeding the FEL process in the BTFEL is briefly investigated in Section 5.

2. The low-energy small-undulator period SASE regime

In the SASE mode, BTFEL will be operated with a relatively low charge per bunch of 50 pC in a bunch length of 500 fs rms to produce a single-spike ~ 2 μm IR radiation with a mega-watt peak power in approximately 4-m saturation length.

Adoption of the short-period undulator at low energies (i.e., few tens of MeV) reveals a few noteworthy beam dynamics and radiation properties.

Indeed in such a regime, the electron beam experiences a unusually strong natural vertical focusing inside the planar undulator.

In addition, the low energy combined with the small emittances of the beam makes space charge forces non-negligible, so that their effects must be accounted in beam dynamics calculations. For example, it will be shown later that additional horizontal focusing between the few undulator modules of the BTFEL needs to be added to avoid that space-charge forces deteriorate the brightness of electron beam.

The small undulator gap (~ 2 mm) combined with the low beam energy, increase the effects on beam dynamics due to nonlinear undulator field components, and can result in effective emittance growth if the beam size at the undulator entrance is too large. Because of that, a careful optics matching at the entrance of the undulator is required, especially in the vertical plane. In our proposed scheme, such matching has been achieved by appropriately choosing the length of the undulator modules to provide a periodic optical solution.

Another noticeable characteristic of this regime is the large slippage length due to the short-period undulator and the rather long radiation wavelength. The resonance condition for an undulator, already discussed in the previous section, implies that the electron beam slips with respect to the radiation pulse exactly one wavelength per each undulator period. Unlike X-ray FELs where the radiation wavelength is many orders of magnitude smaller, the slippage length for IR FELs is rather large so that the radiation pulse can 'escape' from the electron beam prematurely if the electron bunch length is not sufficiently long with a negative impact on the FEL performance.

3. Electron-beam and radiation properties

In the FEL process, the amplification of the electromagnetic (EM) wave is due to the collective instability in the electron beam. The instability produces an exponential growth of the EM field intensity and of the bunching at the radiation wavelength given by the bunching parameter

$$B = \frac{1}{N_e}\sum_{k=1}^{N_e} \exp\left(\frac{2\pi i}{\lambda} z_k\right) \tag{1}$$

where z_k is the longitudinal position of the kth electron with respect to the bunch center, N_e is the total number of electrons and $i=\sqrt{-1}$. The growth saturates when the bunching parameter modulus is of order unity. In the one-dimensional limit, the power growth before saturation is given by [10]

$$P \approx \frac{1}{9} P_n \exp\left(\frac{z}{L_{g,1d}}\right) \tag{2}$$

where $L_{g,1d} \approx \lambda_u/4\sqrt{3}\pi\rho$ is the one-dimensional power gain length, P_n is the effective input noise power associated with modulations in the instantaneous current, and ρ is the FEL parameter [9] defined as

$$\rho = \left(\frac{1}{16}\frac{I}{I_A}\frac{K^2[JJ(\chi)]^2}{\gamma^3\sigma_x^2 k_u^2}\right)^{1/3} \approx \frac{0.136}{\gamma} J^{1/3} B_u^{2/3} \lambda_u^{4/3} \tag{3}$$

here, I is the peak current of the electron beam, $I_A \approx 17$ kA is the Alfvén current, σ_x is the rms beam size of the electron beam, $k_u = 2\pi/\lambda_u$, and $J = en_e\beta c$ is the electron current density with n_e being the electron density. The function $JJ(\chi)$ measures the coupling between the electron beam and the radiation. For a planar undulator it is given by $JJ(\chi) = J_0(\chi) - J_1(\chi)$, where $\chi = K^2/4(1+K^2/2)$ and J_n is the nth-order Bessel function. The radiated energy at saturation is roughly $\rho N_e E_e$ with E_e being the kinetic energy of an electron.

When three-dimensional effects are considered, the gain length L_g can be expressed in terms of the 1D gain length $L_{g,1d}$ and by introducing the universal scaling function Λ such that

$$L_g = L_{g,1d}(1 + \Lambda(\eta_d, \eta_\varepsilon, \eta_\gamma)) \tag{4}$$

where

$$\eta_d = \frac{L_{g,1d}}{2k\sigma_x^2} = \frac{L_{g,1d}}{Z_R}, \quad \eta_\varepsilon = \left(\frac{L_{g,1d}}{\beta_F}\right)\left(\frac{4\pi\varepsilon}{\lambda}\right)$$

$$\eta_\gamma = 4\pi\left(\frac{L_{g,1d}}{\lambda_u}\right)\left(\frac{\sigma_\gamma}{\gamma}\right). \tag{5}$$

In the above equations, η_d is the diffraction parameter, η_ε is the angular spread parameter, and η_γ is the energy spread parameter. In addition, $k=2\pi/\lambda$, Z_R is the Rayleigh length, β_F is the transverse beta function and $\varepsilon=\varepsilon_n/\beta\gamma$ is the transverse geometric emittance. These scaling parameters measure the deviation of the beam from ideal 1D case. Xie fitted the function Λ numerically and listed the fitting coefficients [11,12]. The saturated power, including 3D effects, obtained by the fitting results is then given by

$$P_{sat} \approx 1.6\rho\left(\frac{L_{g,1d}}{L_g}\right)^2 P_{beam} \tag{6}$$

where P_{beam} is the electron-beam power.

Table 1 shows the FEL parameters for the BTFEL obtained from the semi-analytical theory described above. The quantities in the table have been calculated with electron beam and undulator parameters that will be discussed in the next subsections. Also, as it will be explained later, due to space charge forces the emittance and energy spread inside the undulator experience some increase. To account for this effect, the FEL quantities in Table 1 have been calculated with $\varepsilon_n=0.5$ μm and an rms energy spread of 30 keV (instead of the 0.4 μm and 20 keV required at the undulator entrance). With such values, the FEL parameter $\rho\sim4.2\times10^{-3}$ and 1D gain length $L_{g,1d}\sim7.5$ cm are obtained, and the 3D-correction function Λ is dominated by the contributions of the diffraction and energy spread terms η_d and η_γ, and assumes a value close to unity generating a still remarkably short 3D gain length L_g of ~15 cm. The Rayleigh length of ~20 cm is significantly longer than that corresponding to the average spot size of the electron beam in the undulator of 90 μm (equivalent to an average β_F of 0.75 m), due to the strong effect of diffraction on the evolution of the radiation pulse. The calculations (and the time-dependent simulations later) show that with such a choice of parameters, a single-spike IR pulse with peak power surpassing 0.5 MW can be generated.

It is important to note that the saturation length and saturation power in the table refer to the steady-state regime where the bunch length is much longer than the cooperation length, and Eqs. (4) and (6) are not strictly applicable [13] to electron bunches as short as in our case. Nevertheless, they will be used as a reference for the time-dependent simulations presented later in the paper.

Table 1
Parameters of the BTF FEL.

Parameter	Value
Radiation wavelength, λ (μm)	1.95
Electron beam energy, E_e (MeV)	23.0
Undulator type	Superconducting tape
Undulator period, λ_u (cm)	0.7
Undulator full gap, g (mm)	~2
Undulator peak field on-axis, B_u (T)	0.91764
Undulator parameter, K	0.6
Normalized rms emittance at undulator entrance, ε_n (μm)	0.4
Peak electron beam current, I (A)	40
Bunch charge, Q (pC)	50
Rms energy spread at undulator entrance, σ_E (keV)	20
Rayleigh length, Z_R (cm)	20
Power gain length (1D), $L_{g,1d}$ (m)	0.076
Power gain length (3D), L_g (m)	0.15
FEL parameter (1-D), ρ	4.2×10^{-3}
Rms bunch length, τ_B (fs)	500
Cooperation length, L_c (μm)	41
Allowed saturation length, L_{sat} (m)	4.3
Saturation power, P_{sat} (MW)	< 1.0

3.1. Electron beam from APEX

The predicted FEL gain length for the BTFEL in the configuration of Table 1 is of 15 cm (including 3D effects). With the 7 mm undulator period that corresponds to a radiation slippage per gain length of ~40 μm, or equivalently to a cooperation length of ~140 fs. In order to approach the performance predicted by steady state calculations, a bunch length several times longer than the cooperation length is required. In the BTF, a bunch length of 500 fs rms at the undulator entrance was selected trading between the FEL performance and a reasonable bunch compression requirement for the APEX injector.

In the solution we adopted, a peak current of 40 A is necessary to achieve the required FEL gain. For a Gaussian distribution with 500 fs rms length that implies a bunch charge of 50 pC. The gradient and output beam energy of the APEX high-repetition rate electron gun (~20 MV/m and 0.75 MeV respectively) requires the use of relatively long bunches at the cathode in order to control emittance dilution due to space charge forces. For the BTFEL case, a trapezoidal bunch with ~15 ps plateau is used to preserve the required normalized emittance of 0.4 μm. The BTFEL layout does not include a magnetic compressor, and bunch compression is performed by a dedicated buncher cavity and by velocity bunching [14] along the first two linac accelerating sections. Velocity bunching requires a significant de-phasing of the RF in the accelerating sections, inducing as a side effect a decrease of the beam energy at the APEX exit from the maximum of ~30 MeV (when all the sections are phased for maximum energy gain) down to ~23 MeV. The FEL calculations indicate that the beam energy spread at the entrance to the undulator must be at or below ~30 keV rms.

Fig. 2 shows simulation results for a possible APEX configuration that generates beam parameters consistent with the requirements of Table 1.

3.2. Superconducting tape undulator

The high-temperature superconductor YBCO ($YBa_2Cu_3O_7$) has a transition temperature of about 120 K and critical fields B_{c2} in excess of 100 T. Very high transport current can be maintained in the material if properly manufactured and operated at cryogenic temperatures.

Tapes with an YBCO core designed for superconducting magnet applications are commercially available at relatively low cost [2]. Available tape cross-sections include many mm in width and 50−100 μm in thickness. The thickness is composed mainly of a strong substrate, typically Hastelloy, that provides mechanical integrity. Buffer layers are then applied to provide a texture for the growth of a $YBa_2Cu_3O_7$ crystal. The YBCO layer is typically ~1 μm thick in commercial tapes, although 2−3 μm thicknesses have been produced in non-commercial lengths.

The critical transport current density J_{sc} in the YBCO layer is a function of temperature, applied magnetic field, and strain. A typical value in commercial tapes is J_{sc} (77 K, 0 T) ~30 kA/mm^2; at 4.2 K the value can increase by a factor of 10 or more. These current densities are much higher (~10) than can be obtained with conventional low-temperature superconductors (LTS). LTS benefit, however, from higher average current densities: the area ratio of superconductor to normal metal in the YBCO tapes is 1–3% as compared to 25–50% for LTS materials.

Using micro-machining or lithography techniques a flat YBCO tape conductor can be machined with grooves that force the current

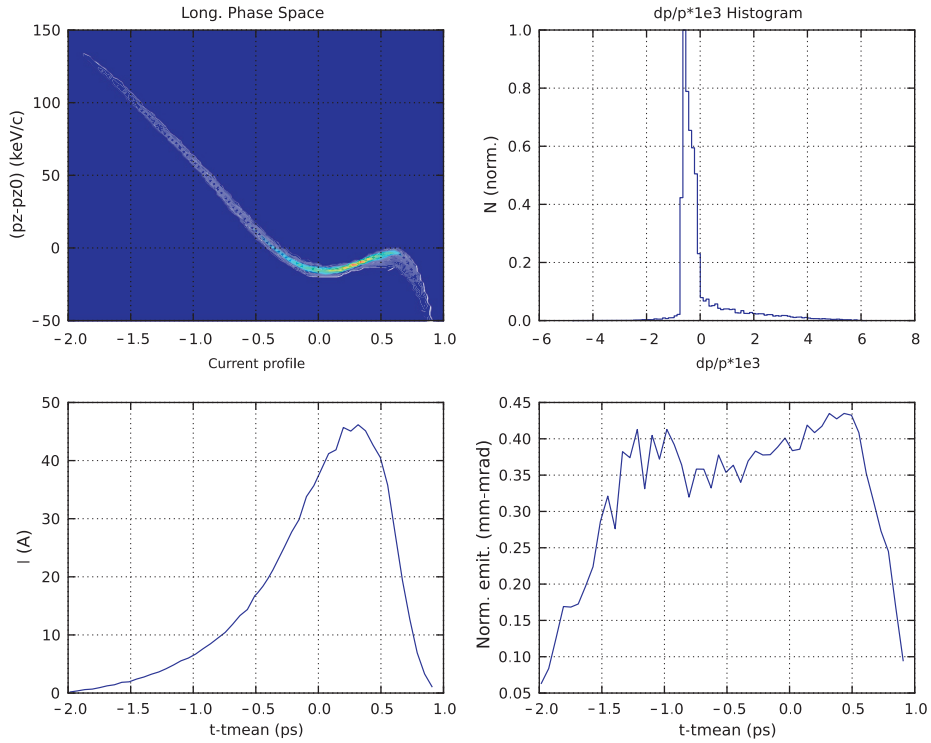

Fig. 2. Phase space distribution at the undulator entrance for a possible APEX beam matching the requirements for BTFEL.

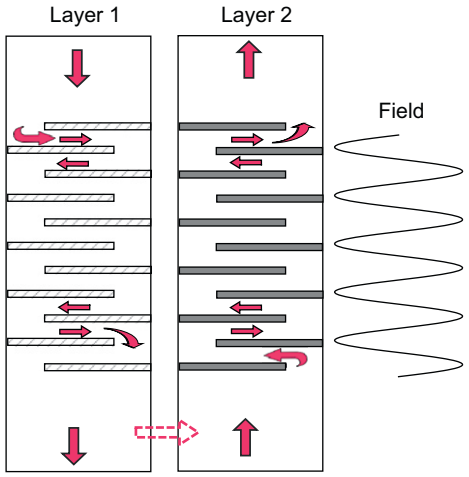

Fig. 3. HTS tape undulator concept, showing current path for two of the many layers making up each half of the undulator. A sketch of the field oscillations as a function of longitudinal position is shown on the right.

in a defined path to obtain the desired undulator field profile. Multiple layers can be super-imposed to yield additional field strength. The basic concept is shown in Fig. 3. For small undulator gaps this approach leverages the tape geometry and high current density of the YBCO superconductor. Lithography, in particular, can provide highly accurate and reproducible periodicity, thereby eliminating a dominant source of field error in short-period undulators. The current passing from one transverse segment (i.e. half-period) to another results in a longitudinal edge current which, for a single tape, results in a quadrupole-like field on the beam axis. In the proposed configuration the next tape in the stack has longitudinal currents flowing in the opposite direction, resulting in a canceling of the quadrupole field. An even number of layers will therefore result in negligible on-axis harmonic content.

Other error sources, such as variations in current distribution in the tape, are under investigation. Note that the undulator does not include magnetic material, thereby facilitating error analysis and correction.

A prototype of such an undulator operating at 4.2 K is under development at LBNL, and has been designed to have a 7 mm undulator period, with a 2 mm gap and a field intensity on the axis of ~ 0.92 T sufficient to achieve an undulator parameter $K \sim 0.6$. A detailed design of the 'cold-mass' has been developed, and a preliminary investigation of tolerances made [4]. Based on the analysis, variations in current distribution from one half period to another will result in phase errors, but not net trajectory (steering or displacement) errors.

The lithography approach has been applied at LBNL to tape samples, yielding patterned components for the prototype device. Transport current measurements have been made at 4.2 K in a liquid helium dewar. The current densities obtained in the samples have been typically on the order $J_{sc} \sim 2 \times 10^5$ A/mm^2, quite sufficient to meet the field requirements. Hall probe measurements at consecutive lithography-patterned cuts clearly demonstrated the expected oscillating field.

A 3D CAD view of the extremely compact 'cold mass' of the undulator prototype is shown in Fig. 4. For reference, the width of the part is ~ 4 cm. The system will likely be cooled in a cryogen-free cryostat, as the I_{sc} is fairly insensitive to small temperature variations about 4.2 K. A test cryostat is currently under design. For field measurements, a pulsed-wire system has been developed that yields accurate first and second integrals of the field as a function of longitudinal position.

With such an undulator and the APEX beam parameters, the BTFEL will radiate at a wavelength of ~ 1.95 μm.

3.3. Optical functions at the undulator

Proper focusing of electron beam is required for an efficient FEL interaction between electrons and radiation. Indeed, if the

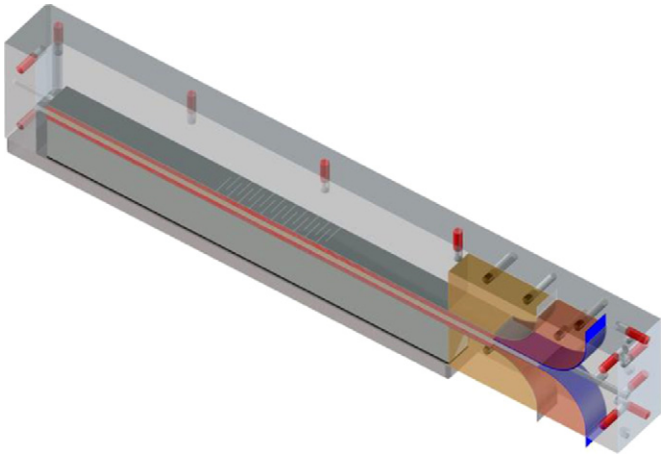

Fig. 4. CAD view of the 'cold mass' of the super-conducting tape undulator. Not shown in the figure the cryostat that contains the part.

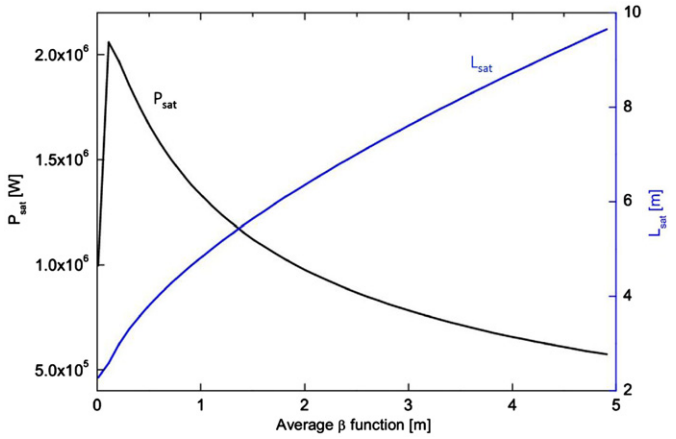

Fig. 5. Radiation power (steady-state) at saturation and saturation length as a function of the average beta function in the undulator. The power is maximum at $\beta \sim 0.2$ m.

beam expands too rapidly, it will limit the radiation power and increase the saturation length. The optimal average beam size (and hence beta function) and its effect on the radiation power and FEL saturation length are now evaluated. Fig. 5 shows the saturation power and saturation length (in steady-state mode) as a function of the average beta function in the undulator, calculated using the semi-analytical model of Section 3. The figure shows the existence of a power maximum at an average beta function of ~ 0.2 m. Note that such results are approximated and used only as an estimation tool. In fact, because of the difference in focusing between the transverse planes, the electron beam through the undulator becomes flat transversely with different beta functions between the horizontal and vertical planes.

The short-period planar undulator together with low-electron energy leads to a remarkably strong natural focusing in the vertical plane and no focusing in the horizontal one. It will be shown in the next subsection that horizontal focusing must be added to control space charge effects inside the undulator. In order to provide such a focusing, the BTFEL undulator is segmented in three modules, and horizontally focusing quadrupoles are inserted between the modules. The length of each segment is chosen to be 1.204 m (i.e., 172 undulator periods) with which a periodic beta function solution exists. Fig. 6 shows the horizontal and vertical beta functions along the undulator for such a solution when no space charge force is applied. It can be seen that, while

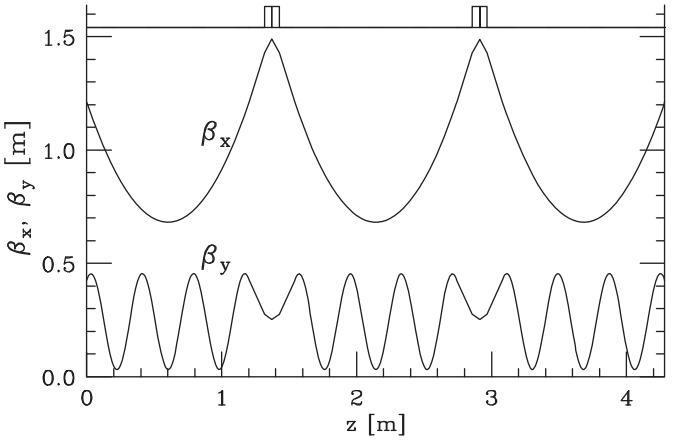

Fig. 6. Betatron functions in the undulator. Two horizontal focusing quadrupoles are placed between 1.2-m long undulators.

the average vertical beta function is close to the optimal value of 0.2 m, the average horizontal beta function is larger than that. To account for such a situation, a tradeoff value of 0.75 m for the average beta function has been used for both planes in the semi-analytical calculations presented in Table 1.

3.4. Space-charge effects

The relatively low-energy of the APEX beam is not sufficient to make space charge forces negligible. In this situation, the lack of horizontal focusing in the undulator results in noticeable space-charge induced increase of emittance and energy spread, while in the vertical plane, the undulator natural focusing is sufficient to overcome the space-charge force.

Such a scenario can be qualitatively understood by using the envelope equations for the case of a continuous beam and linear space charge forces [15]

$$X'' + k_x X - \frac{2K_{sc}}{X+Y} - \frac{\varepsilon_x^2}{X^3} = 0$$

$$Y'' + k_y Y - \frac{2K_{sc}}{X+Y} - \frac{\varepsilon_y^2}{Y^3} = 0 \tag{7}$$

where X and Y are the horizontal and vertical beam envelopes, $k_y = (\sqrt{2}\pi K/\lambda_u\gamma)^2$ and $k_x = 0$ are respectively the undulator vertical and horizontal focusing strengths (in the absence of quadrupoles), and $K_{sc} \approx 1.174 \times 10^{-4} I/\gamma^3$ is the space charge parameter. Using the values at the entrance of the BTFEL undulator for the relevant quantities in the above equations, one can find that in the vertical plane, the undulator focusing term ($\sim 4.2 \times 10^{-3}$ m^{-1}) is greater than the space-charge ($\sim 5.9 \times 10^{-4}$ m^{-1}) and emittance ($\sim 3.4 \times 10^{-4}$ m^{-1}) terms, and large enough to control space charge effects. That is not the case for the horizontal plane due to the absence of horizontal focusing.

To the authors' knowledge, existing FEL codes do not take into account transverse space-charge effects. Such codes are mainly designed for short-wavelength radiation where transverse space-charge forces ($\propto \gamma^{-2}$) can be neglected because of the larger beam energy. Because of this, to examine the effects of space charge in the BTFEL undulators more quantitatively, the electron beam tracking code PARMELA [16] was used. It should be remarked that the results of the simulations with PARMELA are only approximated because the longitudinal micro-bunching induced by the SASE process is not included, and they were used only for estimating the space charge effects on emittance and energy spread.

The undulator field was modeled by

$$B_x = 0, \quad B_y = B_u \cosh k_u y \cos k_u z$$

$$B_z = -B_u \sinh k_u y \sin k_u z \tag{8}$$

where $k_u = 2\pi/\lambda_u$. End field corrections were applied to make the first and second field integrals along the undulator vanish.

Fig. 7 shows the horizontal and vertical beta functions in the presence of space charge calculated by PARMELA using 200 thousand particles and after some re-adjustment of the quadrupole strengths. Comparing with Fig. 6, the presence of a noticeable distortion in β_x can be observed, while β_y remains reasonably close to the no space-charge case.

Fig. 8 shows the variation of the normalized transverse emittance along the undulators, calculated using the beam distributions at the different $z$positions. The horizontal emittance initially increases, reaches a maximum of ~ 0.45 μm in the center, and then, under the action of the horizontally focusing quadrupoles, decreases back to ~ 0.42 μm at the undulator exit, just $\sim 5\%$ above the value at the entrance of the undulator entrance. The vertical emittance experiences a more moderate increase probably also due to the nonlinear field components of the undulator as shown in Eq. (8).

The rms energy spread increases significantly due to space-charge forces (see Fig. 9), whereas the increase in the rms bunch length is essentially negligible (see Fig. 10).

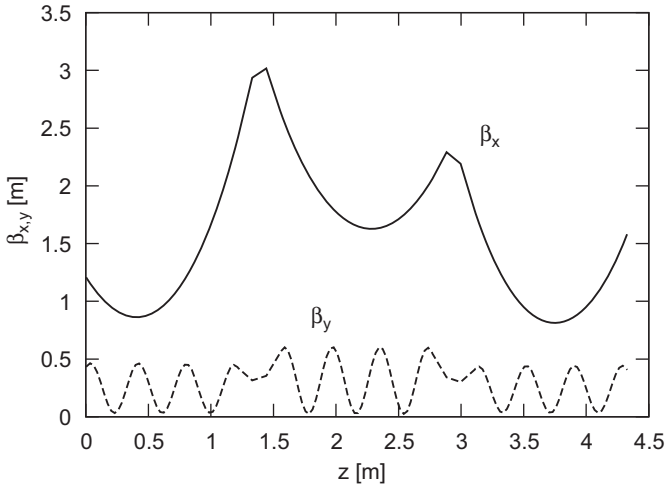

Fig. 7. Change in beta functions in the undulator in the presence of space charge effect.

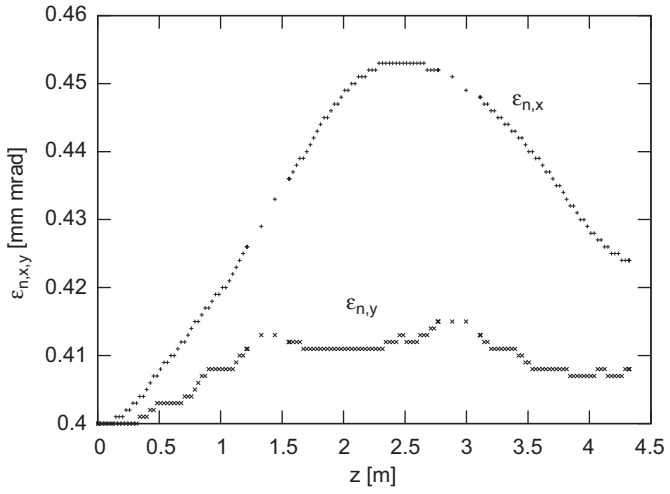

Fig. 8. Variation of the horizontal and vertical normalized emittances in the undulator in the presence of space charge effect.

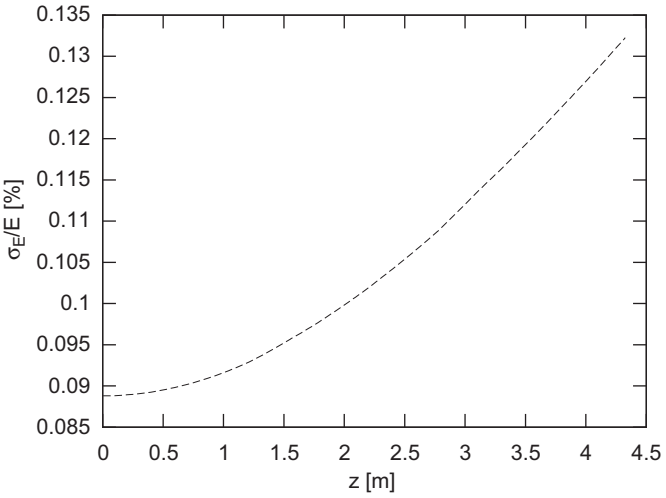

Fig. 9. Variation of the rms energy spread (relative) in the undulator in the presence of space charge effect.

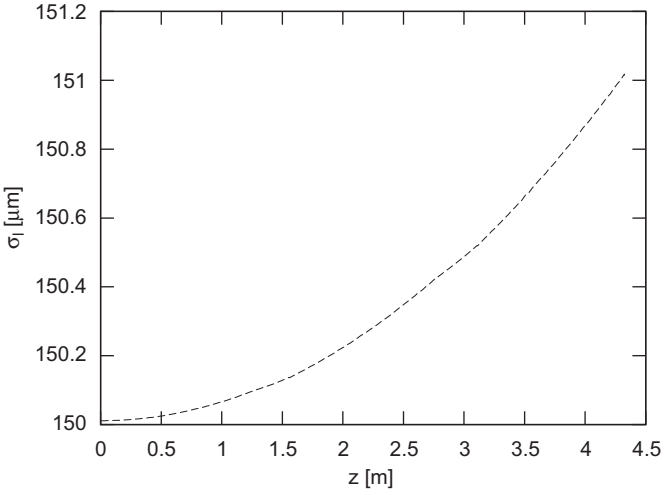

Fig. 10. Variation of the rms bunch length in the undulator in the presence of space charge effect.

4. Time-dependent simulations

For an efficient FEL interaction, the Rayleigh length $Z_R \equiv 4\pi\sigma_x^2/\lambda$ should be sufficiently larger than the gain length to make diffraction effects negligible. However, as discussed in Section 3, this is not the case for the BTFEL where the long wavelength and the strong natural focusing of the undulator yield to a rather short Rayleigh length (see Table 1).

In addition, as also discussed in Section 3, the bunch length in the BTFEL is just few times longer than the cooperation length and the steady-state solutions are only approximated and need to be validated.

Last but not least, the single-spike characteristic of the BTFEL IR pulse needs to be verified as well.

Therefore, three-dimensional time-dependent simulations were required and the FEL code GENESIS [17] has been utilized for the scope.

In the previous section, it has been shown that the high-brightness electron beam in the BTFEL experiences non-negligible space-charge forces that increase the beam transverse emittance and energy spread. For accounting for this effect, in the evaluation

of the quantities in Table 1, and also in the following simulations the larger values of 0.5 μm and 30 keV have been assumed for the normalized emittance and for the rms energy spread respectively. Such values are significantly higher than the respective ones at the undulator entrance (+25% for the emittance and +50% for the energy spread), and should allow for a conservative accounting of space charge effects.

The curve (a) in Fig. 11 shows the IR radiation power along the photon pulse at distance of ~4.3 m from the undulator entrance simulated with GENESIS using the values discussed above. A clean single-spike structure is clearly visible, with a peak power of 0.6 MW corresponding to a radiation pulse of ~0.4 μJ. As a comparison, the curve (b) in the same figure shows the case for the same energy spread but with an increased emittance value of 0.6 μm. In such a case, the peak power of the single-spike radiation drops by a factor of more than a half. The current profile is shown in curve (c), against the right-hand scale.

Fig. 12 shows instead the dependence of peak power for $\varepsilon_n = 0.5$ μm on the value of σ_E. The solid portion of the curve corresponds to a single spike pulse, while the dashed portion corresponds to multiple spikes. Although a reasonable single spike pulse is still generated up to energy spreads of 40 keV, the peak power drops drastically down to noise levels. This indicates a stronger sensitivity of the radiation power to the energy spread compared to the predictions of the 3D calculations in Section 3. In addition to the usual effect of the distance to saturation lengthening as the energy spread is increased, the ratio of the cooperation length to the electron bunch length eventually becomes too small to support significant gain, as slippage convects the radiation out of the electron bunch too rapidly. It must be remarked that after accounting for this dependence of the radiation power on the energy spread, the overall the time-dependent simulation results are in good agreement with the steady-state calculations presented in Table 1.

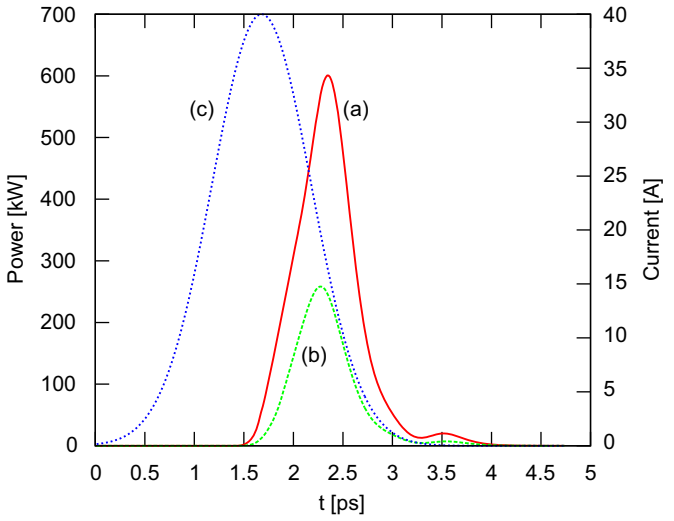

Fig. 11. Radiation power at $z=4.3$ m from the entrance of the undulator for: (a) $\varepsilon_n = 0.5$ μm and $\sigma_E = 30$ keV; (b) $\varepsilon_n = 0.6$ μm and $\sigma_E = 30$ keV. The current profile (c) is shown as well, scaled to the right-hand axis.

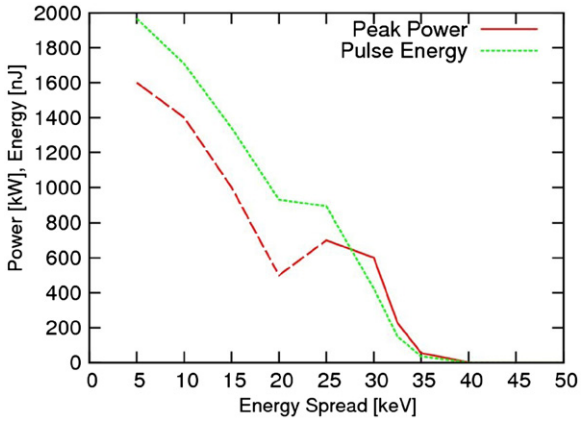

Fig. 12. Typical peak power (solid/dashed line) and pulse energy (dotted line) at $z=4.3$ m from the entrance of the undulator for $\varepsilon_n = 0.5$ μm as a function of energy spread. The dashed portion of the power curve corresponds to multiple spikes in the output, rather than a single peak.

The radiation mode size in the BTFEL is rather large compared to the electron beam transverse size as indicated by the large diffraction term ($\eta_d > 1$ in Eq. (5)). In the large diffraction regime, multiple transverse modes can be excited in the initial start-up stage, but the fundamental mode has the largest growth rate and, at a certain longitudinal position, will dominate the exponential growth, and the radiation pulse will eventually exhibit a single transverse mode. Such a behavior is confirmed by the time-dependent simulations. Fig. 13 shows the transverse radiation profiles resulting from such simulations at various positions along the undulator. A clean single mode transverse profile is visible at $z=4.3$ m.

5. BTFEL laser seeding

The SASE process starts from noise (small random density modulations along the bunch) and therefore the micro-bunching process evolves rather slowly requiring a quite long undulator system for achieving saturation. If a laser beam, co-propagating with the electron beam inside the undulator, is used for imposing an energy modulation on the electron bunch and hence seeding the micro-bunching, the whole process can occur more rapidly and saturation can be achieved within significantly shorter undulators.

Fig. 14 shows the GENESIS-simulated average-power evolution of the radiation over the undulator length, when seeding the BTFEL electron beam ($\sigma_z = 500$ fs, $\varepsilon_n = 0.5$ μm, and $\sigma_E = 30$ keV) with a 100 fs IR laser pulse with 10 kW peak power. Commercial laser systems with those characteristics (2.5 nJ per pulse) are readily available. The power in the figure is averaged over all the longitudinal bunch slices (seeded and un-seeded) and shows saturation at $z \sim 1.2$ m. Fig. 15 shows the resulting single-spike radiation at various distances from the undulator entrance. The current profile is as in Fig. 11. We remark that the original laser pulse itself does not become amplified, but instead leaves behind an enhanced bunching which subsequently radiates a much stronger second pulse.

This preliminary and initial investigation indicates that it is plausible to obtain saturation and a single-spike radiation pulse in 1.2 m with a reasonable seeding. There is a wide range of options to consider in order to optimize the seeded configuration, such as varying the bunch charge or the duration of the laser seed. Pursuing such tasks requires further work and is not the subject of this paper.

6. Conclusions

The possibility of testing a sub-cm period novel-design undulator based on a commercial super-conducting tape, with the APEX high-brightness electron beam has been investigated.

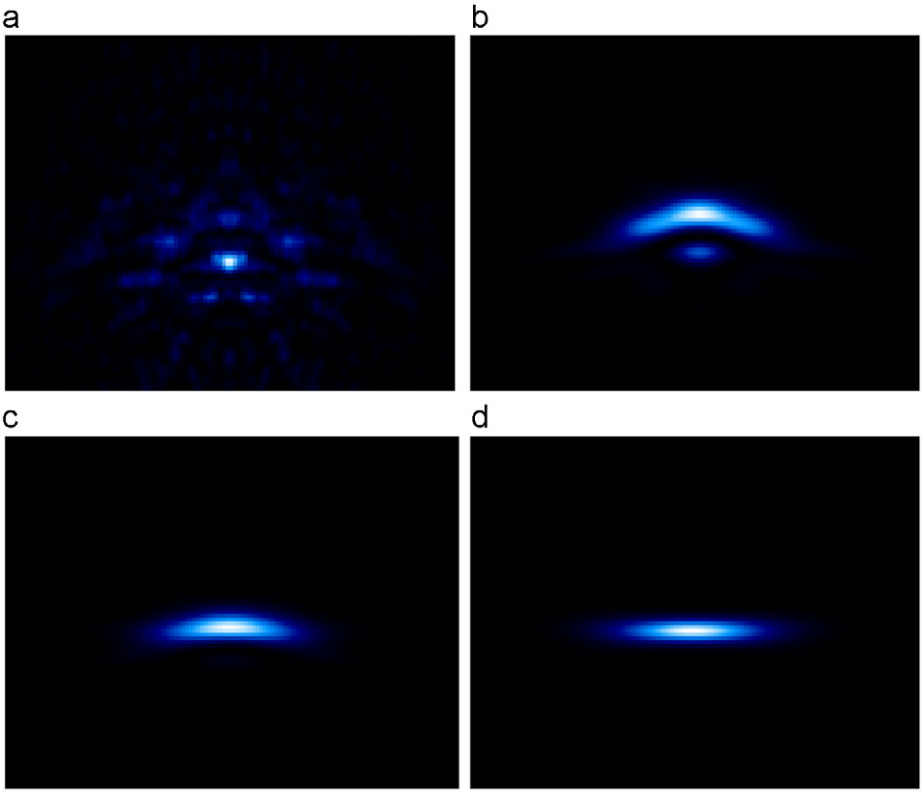

Fig. 13. (Unscaled) Transverse profile of the radiation from BTF FEL at (a) z=0.6 m, (b) z=1.75 m, (c) z=2.4 m and (d) z=4.3 m.

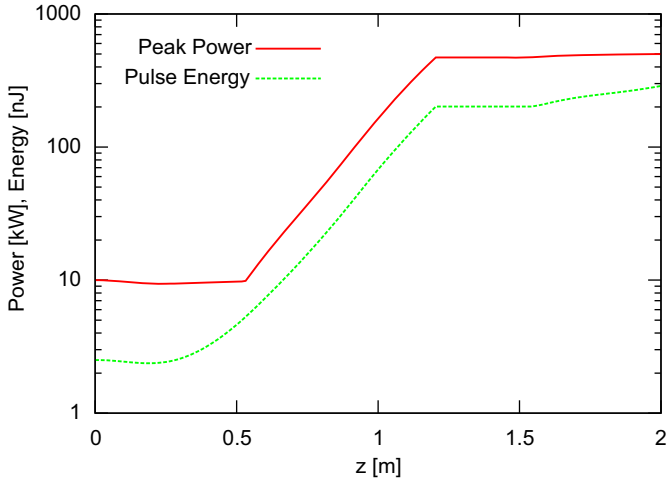

Fig. 14. Evolution of the peak power and total energy per pulse for $\varepsilon_n = 0.5$ μm and $\sigma_E = 30$ keV seeded by a 10 kW, 100 fs laser.

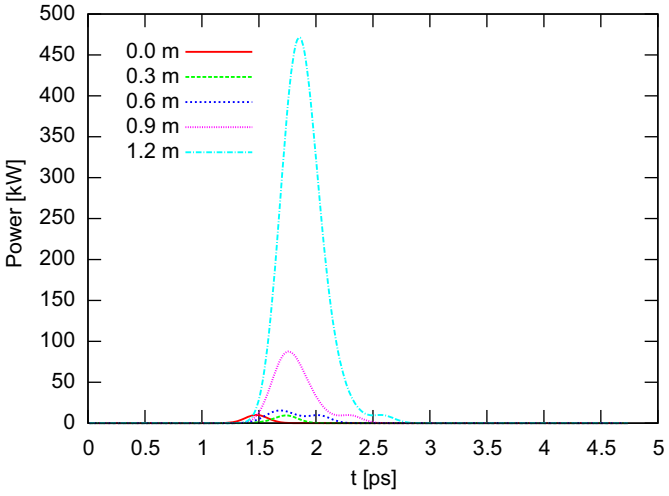

Fig. 15. Radiation power at various distances from the entrance of the undulator for $\varepsilon_n = 0.5$ μm and $\sigma_E = 30$ keV seeded by a 10 kW, 100 fs laser.

The combination of the two generates the BTFEL, an infrared SASE FEL lasing at ~2 μm in a single-spike radiation pulse with ~0.6 MW peak power saturating in ~4 m. The low energy of the APEX electron beam (few tens of MeV) jointly with the short undulator period forces the FEL in a regime with unusual and interesting characteristics.

3D calculations and time-dependent simulations describing the BTFEL performance were presented including an initial evaluation of a promising laser seeding option offering saturation in ~1.2 m.

Future planned studies include start to end simulation of the BTFEL dynamics, and the evaluation of the effects of wakefields on the FEL performance. In particular, the superconducting undulator requires the investigation of the effect of resistive wall wakefields in the anomalous skin effect regime [18].

Acknowledgments

The authors want to thank Max Zolotorev for useful discussion and suggestions. This work was supported by the Director of the Office of Science of the U.S. Department of Energy under Contract no. DE-AC02-05CH11231.

References

[1] P. Emma, R. Akre, J. Arthur, R. Bionta, C. Bostedt, J. Bozek, A. Brachmann, P. Bucksbaum, R. Coffee, F.-J. Decker, Y. Ding, D. Dowell, S. Edstrom, A. Fisher, J. Frisch, S. Gilevich, J. Hastings, G. Hays, Ph. Hering, Z. Huang, R. Iverson, H. Loos, M. Messerschmidt, A. Miahnahri, S. Moeller, H.-D. Nuhn, G. Pile,

D. Ratner, J. Rzepiela, D. Schultz, T. Smith, P. Stefan, H. Tompkins, J. Turner, J. Welch, W. White, J. Wu, G. Yocky, J. Galayda, Nature Photonics 4 (2010) 641.
[2] P. Lee, available at 〈http://www.magnet.fsu.edu/magnettechnology/research/asc/plots.html〉.
[3] S. Prestemon, D. Dietderich, A. Madur, S. Marks, R.D. Schlueter, High performance short-period undulators using high temperature superconductor tapes, in: Proceedings of the 2009 Particle Accelerator Conference, Vancouver, BC, Canada, 2009, pp. 2438–2440.
[4] S. Prestemon, D. Arbelaez, S. Davies, D.R. Dietderich, D. Lee, F. Minervini, R.D. Schlueter, IEEE Transactions on Applied Superconductivity 21 (3) (2011).
[5] J. Staples, F. Sannibale, S. Virostek, VHF-Band Photoinjector, CBP Technical Note 366, 2006.
[6] K. Baptiste, J. Corlett, S. Kwiatkowski, S. Lidia, J. Qiang, F. Sannibale, K. Sonnad, J. Staples, S. Virostek, R. Wells, Nuclear Instruments and Methods in Physics Research Section A 599 (2009) 9.
[7] F. Sannibale, B. Bailey, K. Baptiste, A. Catalano, D. Colomb, J. Corlett, S. De Santis, L. Doolittle, J. Feng, D. Filippetto, G. Huang, R. Kraft, D. Li, M. Messerly, H. Padmore, C.F. Papadopoulos, G. Portmann, M. Prantil, S. Prestemon, J. Qiang, J. Staples, M. Stuart, T. Vecchione, R. Wells, M. Yoon, M. Zolotorev, Status of the LBNL normal-conducting CW VHF electron photo-gun, in: Proceedings of the 2010 FEL Conference, Malmö, Sweden, 23–27 August 2010, pp. 475–478.
[8] A. Kondratenko, E. Saldin, Particle Accelerators 10 (1980) 207.
[9] R. Bonifacio, C. Pellegrini, L.M. Narducci, Optics Communications 50 (1984) 373.
[10] See for example Z. Huang, K.-J. Kim, Physical Review Special Topics—Accelerators and Beams 10 (2007) 034801.
[11] M. Xie, Design optimization for an X-ray free electron laser driven by SLAC linac, in: Proceedings of the 1995 Particle Accelerator Conference, Dallas TX, USA, 1995, pp. 183–185.
[12] M. Xie, Nuclear Instruments and Methods in Physics Research Section A 445 (2000) 59 (Piscataway, NJ, 1995, p. 183).
[13] R. Bonifacio, L. De Salvo, P. Pierini, N. Piovella, C. Pellegrini, Physical Review Letters 73 (1994) 70.
[14] L. Serafini, M. Ferrario, AIP Conference Proceedings 581 (2001) 87.
[15] See for example: M. Reiser, Theory and Design of Charged Particle Beams, Wiley-Vch Editor, 2008 ISBN 978-3-527-40741-5.
[16] L.M. Young, PARMELA, LA-UR-96-1835, Revised December 1, 2005.
[17] S. Reiche, Nuclear Instruments and Methods in Physics Research Section A 429 (1999) 243.
[18] B. Podobedov, Physical Review Special Topics—Accelerators and Beams 12 (2009) 044401.